Pergamon

Acta mater. 48 (2000) 4517–4530

Acta MATERIALIA

www.elsevier.com/locate/actamat

AN *AB INITIO* STUDY OF THE CLEAVAGE ANISOTROPY IN SILICON

R. PÉREZ[1,2] **and P. GUMBSCH**[2]*

[1]Departamento de Física Teórica de la Materia Condensada, Universidad Autónoma de Madrid, E-28049 Madrid, Spain and [2]Max-Planck-Institut für Metallforschung, Seestrasse 92, 70174 Stuttgart, Germany

Abstract—Total-energy pseudopotential calculations are used to study the cleavage fracture processes in silicon. It is shown that bonds break continuously and cracks propagate easily on {111} and {110} planes provided crack propagation proceeds in the ⟨110⟩ direction. In contrast, if the crack is driven in a ⟨001⟩ direction on a {110} plane the bond breaking process is discontinuous and associated with pronounced relaxations of the surrounding atoms. The discontinuous process is partly a result of some load sharing between the crack tip bond and the neighbouring bond, which results in a large lattice trapping. The different lattice trapping for different crack propagation directions can explain the experimentally observed cleavage anisotropy in silicon single crystals. *© 2000 Acta Metallurgica Inc. Published by Elsevier Science Ltd. All rights reserved.*

Keywords: *Ab initio* calculation; Elemental semiconductors; Mechanical properties; Brittle fracture; Theory and modelling, defects

1. INTRODUCTION

The macroscopic failure of materials is ultimately determined by events on the atomic scale. This is particularly clear in the case of brittle fracture, where the crack at its tip must be atomically sharp and break the bonds between atoms. Such a brittle crack can therefore be regarded as a macroscopic probe for the atomic bonding.

Following Griffith [1], one may regard the static crack as a reversible thermodynamic system for which one seeks equilibrium. This equilibrium condition leads to the so-called Griffith criterion, which balances the mechanical energy release upon crack advance $\mathcal{G}$ with the energy required to create the two new surfaces 2γ. Although the Griffith criterion, $\mathcal{G} = 2\gamma$, is often regarded as a fracture criterion, it is important to note that it is only a necessary condition for fracture and not sufficient. Nevertheless the Griffith criterion leads to two important conclusions: (1) crystal lattice planes with low surface energies are energetically favoured as cleavage planes, and (2) a given cleavage plane will have a single unique value of $\mathcal{G}$. A perfectly brittle crack in a crystal is therefore expected to choose a cleavage plane with low surface energy and to propagate on this plane with equal ease in all directions.

From an atomistic point of view the situation is somewhat different. The first atomistic studies showed that the discreteness of the lattice manifests itself in the so-called lattice trapping effect [2, 3]. In a crude continuum analogy, lattice trapping can be interpreted as if the surface energy was oscillating with a period of the atomic distance. Lattice trapping causes the crack to remain stable and not to advance/heal until loads somewhat larger/smaller than the Griffith load are reached. It has been shown that the magnitude of the lattice trapping effect strongly changes with the bonding characteristics [3–6]. Later studies showed that the lattice trapping may even depend on the direction in which the bonds are broken and therefore be very different for crack propagation along different crystallographic directions on one cleavage plane [7–9].

Semiconductors, particularly silicon, are materials that may be suitable to test the perfectly brittle case experimentally. Silicon can be produced as a virtually dislocation-free single crystal and crack tips have been observed in the transmission electron microscope to propagate in the absence of dislocations [10, pp. 79–142]. Silicon has been studied extensively for its fracture characteristics [11–15]. The results of these studies are summarized for example in [16]. In

* To whom all correspondence should be addressed. Fax: 0049 711 2095120.

E-mail address: gumbsch@finix.mpi-stuttgart.mpg.de (P. Gumbsch)

PII: S1359-6454(00)00238-X

short, silicon is reported to have two principal cleavage planes: {111} planes, usually the easy cleavage planes [16], and {110} planes, the planes of easy cleavage in polar III–V semiconductors [14–17], which in silicon can only be obtained under specific conditions for the propagation direction [14]. It is not clear which of the planes has the lower fracture toughness K. The most accurate constant-K experiments [14] seem to show that {110} planes have a slightly lower fracture toughness ($K^c_{110} = 0.89$ MPa$\sqrt{\text{m}}$) than {111} planes ($K^c_{111} = 0.92$ MPa$\sqrt{\text{m}}$). Different crack propagation directions have been studied for both crack planes: the ⟨110⟩ and ⟨211⟩ directions for {111} cleavage and the ⟨110⟩ and ⟨111⟩ directions for {110} cleavage [16]. The ⟨110⟩ propagation direction was seen to be the easy propagation direction for both cleavage planes. One orientation which was not reported in [16], the ⟨100⟩ propagation direction on the {110} plane, could not be cleaved [9]; the cracks were observed to deflect out of the {110} onto the {111} planes. This indicates a very strong cleavage anisotropy with respect to the propagation direction on the same cleavage plane. Such an anisotropy has also been reported for cleavage fracture in tungsten single crystals [8].

Atomistic modelling of cracks is a rather complicated problem because both the long range linear elastic interaction, characterized by the $1/\sqrt{R}$ singularity in the stress field, and the short-range chemical interactions, which are responsible for the atomic scale breaking of bonds at the crack tip, are needed for a correct description of the problem. Changes of the atomic positions at the crack tip will be carried far away by the weak singularity. To properly handle the boundary conditions for the atomistic region, several schemes which combine an atomistic region with a flexible continuum region have been developed [7, 18–20]. The boundary conditions from the field of an elastic crack can then be imposed on the outer border of this continuum region. Apart from the difficulties involved in the transition between the lattice and the continuum and the application of the boundary conditions, the description of the interactions in the atomistic region is a problem in itself. The large number of atoms involved requires a simple and computationally efficient description of the atomic interaction. Therefore, empirical atomic potentials are usually used for fracture simulations. These empirical interatomic potentials are fitted to bulk properties and may then reproduce these properties well. However, the atomic coordination close to the crack tip differs substantially from the bulk environment. The applicability of these empirical potentials for crack simulations is therefore, at least, questionable.

Recently, Holland and Marder [21] have demonstrated very clearly the limits of these empirical descriptions for the application in fracture simulations: they had to manipulate the three-body term of the Si Stillinger–Weber potential [22] in order to obtain crack propagation in Si in their molecular dynamics simulations. Of course, this introduced unwanted changes to the bulk properties of the potential. We have experienced similar problems in our attempt to simulate crack propagation in Si with the Tersoff potential [23]. Despite the fact that this potential is apparently able to describe structures with atomic coordination quite different from the bulk diamond lattice, like surface reconstructions, our simulations showed unphysical structural transitions at the crack tip. These are attributed to the extremely short-range character of the interaction.

In the absence of a simple and yet reliable model for the interaction, two different approaches can be followed. One way is to retain a large atomistic region and treat the atomic interaction as a free parameter which can be modified in order to identify the relevant features that influence crack propagation. Alternatively, one can compromise on the size of the system and concentrate on the quality of the description of the atomic interaction. Total-energy pseudopotential methods, based on density functional theory (DFT) and the use of a plane-wave basis set, have been known since the early 1980s to provide a very accurate description of the structural and energetic properties of solids. The size of the systems that one could study with those methods was limited to tens of atoms, mainly due to the poor system size scaling of the time needed for the diagonalization of the hamiltonian. Recent methodological advances, in particular the development of iterative minimization techniques [24], and the use of parallel computers have now made it possible to study systems containing hundreds of atoms with quantum mechanical methods. This opened the way to extend the applicability of quantum mechanical methods to the study of the mechanical properties of materials. Taking advantage of these methods it is today possible to study the structure of the crack tip during crack propagation using *ab initio* methods to describe the atomic interactions.

The purpose of this paper is to follow this second route and to analyse in detail the bond breaking processes at crack tips in silicon. The analysis is based on ab initio methods which can accurately describe the non-linear forces acting on the crack tip atoms. A full quantum mechanical study is necessary to capture the details of the bond breaking process and of the subsequent reconstructions of the internal surfaces of the crack. Earlier work along this same direction was reported by Spence *et al.* [25]. They used a non-self-consistent *ab initio* tight-binding method to study the lattice trapping for cracks on the (111) plane with a $[0\bar{1}1]$ front. In our case, more elaborate total energy pseudopotential methods [24] are used to study different propagation directions on the (111) and (110) cleavage planes. A fixed boundary approach is used to enforce the elastic boundary conditions representing the crack field. Particular attention is payed to the influence of the fixed boundary by studying the

scaling of the results with system size and the changes with the relative position of the singularity in the elastic field of the crack and the atomic position of the crack tip. We have also determined the surface energies, γ, for the (111) and (110) cleavage planes. To the best of our knowledge, this is the first calculation using first-principles methods of this key ingredient in the analysis of the crack stability.

The results presented here, although limited by the approximations made, provide a basic understanding of several experimental features of crack propagation in Si. In particular, they show that lattice trapping is important for crack propagation and that lattice trapping provides a straightforward explanation for the experimentally observed anisotropy with respect to propagation direction. These detailed studies may further be used to guide the development of simpler semi-empirical atomic interaction models, which have so far failed to give an accurate description of the crack tip.

The rest of paper is organized as follows: Section 2 is devoted to the description of the different crack systems, the model used to describe the cracks with *ab initio* methods, and the procedure we use for the determination of the lattice trapping range. Section 3 presents the structural and energetic properties of both bulk and low-index Si surfaces, with special attention to the determination of the surface energies obtained with our pseudopotential. The results for the stability of the different crack orientations are introduced in Section 4 and their relevance to the understanding of the experimental results is discussed in Section 5. The main conclusions and the perspectives for future work are summarized in Section 6.

2. METHODOLOGY

2.1. Crack geometry

The goal of this study is to determine the stability of cracks with different propagation directions on the (111) and (110) cleavage planes. In particular, the (110) cracks with [001] and [$1\bar{1}0$] fronts ([$1\bar{1}0$] and [001] propagation directions, respectively) and the (111) crack with a [$0\bar{1}1$] front ([$\bar{2}11$] propagation direction) are considered. In the following, the crystallographic orientation of the crack system is specified by the orientation of the crack plane and of the crack front as: (plane)[front].

To study crack tips atomistically it is necessary to provide the atomistic region with the appropriate boundary conditions from the elastic field of the crack. Within linear elastic continuum theory, a sharp straight crack is characterized by the stress field σ and the displacement field u:

$$\sigma_\nu = \frac{K_{\mathrm{M}}}{\sqrt{R}}\alpha_\nu^{\mathrm{M}}(\Theta) \tag{1}$$

$$u_\nu = K_{\mathrm{M}}\sqrt{R}\beta_\nu^{\mathrm{M}}(\Theta) \tag{2}$$

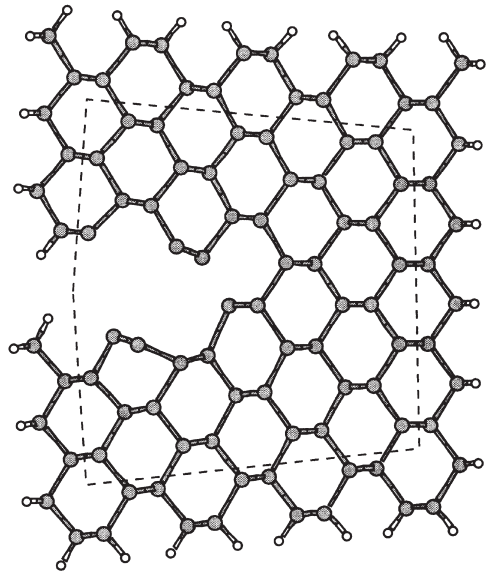

Fig. 1. Illustration of the boundary conditions used in our simulations. The atoms outside of the dashed line are kept fixed during the relaxation process, while the inner atoms are included in the atomic relaxation.

where R is the distance from the crack tip. ν labels the different stress components and M stands for the opening, the shearing or the tearing mode of loading. α and β are functions of the angle Θ between $\vec{R}$ and the crack plane; they further include the crystallographic orientation of the crack system via the appropriate elastic constants. The functions α and β are calculated within anisotropic linear elasticity theory [26]. The applied external load and the geometry of the crack are contained within a single multiplicative factor, the stress intensity factor K_{M}, which thereby characterizes the "strength" of the stress field. More details about the stress field and the energetics of the crack are given in Section 2.3.

The starting configuration of the atoms is given by the anisotropic elastic displacement field for the starting stress intensity factor $K_{\mathrm{I}}^{\mathrm{in}}$. Only mode I (opening mode) loading is considered here. The atomistic region around the crack tip has dangling bonds at the outer surface. These dangling bonds are saturated with H atoms, as shown in Fig. 1 for the (110) crack with a [$1\bar{1}0$] front. It was found that all the bonds of Si atoms which are partially saturated with hydrogen atoms are somewhat less stiff than the bulk Si–Si bonds. Therefore, not only the outermost Si atoms but the positions of the outermost two layers of Si atoms are kept fixed at the positions given by the linear elastic solution (see Fig. 1). The other atoms are relaxed using a conjugate gradient minimization and an ab initio method to determine the total energy and the forces. The system is relaxed until a stable crack tip structure is obtained.

Table 1. Relevant crystallographic information for the different crack systems considered. The crystallographic orientation of the crack systems is given together with the dimensions in the propagation direction, normal to the crack plane and along the crack front (in units of the bulk lattice parameter for the eight-atom simple cubic cell), the number of Si and H atoms in the unit cell, and the extra length (in Å) added to the dimensions in the propagation direction and normal to the crack plane to determine the supercell lattice vectors

Crack orientation (plane)[front]	Dimensions	No. of atoms Si+H	Vacuum size (Å)
(110)[1$\bar{1}$0] small	$6/2 \times 2\sqrt{2} \times \sqrt{2}/2$	48 + 30	10, 14
(110)[1$\bar{1}$0] medium	$7/2 \times 5/2\sqrt{2} \times \sqrt{2}/2$	68 + 34	9, 13
(110)[110] large	$8/2 \times 6/2\sqrt{2} \times \sqrt{2}/2$	96 + 42	11, 14
(110)[001] medium	$2\sqrt{2} \times 2\sqrt{2} \times 1$	64 + 32	9, 14
(110)[00$\bar{1}$] large	$3\sqrt{2} \times 3\sqrt{2} \times 1$	144 + 48	9, 14
(111)[0$\bar{1}$1] medium	$3/2\sqrt{6} \times 2\sqrt{3} \times \sqrt{2}$	70 + 26	10,13

Periodic boundary conditions are applied along the crack front direction to simulate plane strain conditions. Periodicity is also enforced both in the crack propagation direction and the loading direction. However, in these directions the supercell size was chosen larger than the size of the atomic system to avoid the interaction between the atoms in neighbouring cells. The supercell size was chosen large enough to assure a distance of more than 10 Å between atoms in the periodic cells even for the largest loads.

To determine the influence of the size of the atomistic region on the stability of the cracks we have studied the variation of the lattice trapping range with system size for the cracks on the (110) plane. Table 1 summarizes the relevant crystallographic information for the different systems we have considered: the dimensions in the propagation direction, normal to the crack plane, and in the direction of the crack front (in units of the bulk cubic lattice parameter) are given together with the number of Si and H atoms in the unit cell, and the extra length added to the dimensions in the propagation direction and normal to the crack plane to determine the supercell lattice vectors. Figures 2 and 3 show the relaxed atomic configurations of the crack tip atoms of all (110) crack systems at a load where all the systems are stable.

The use of fixed boundary conditions for the atomistic region may affect the stability range of the crack because the elastic field is not allowed to readjust to the changes in the atomic coordinates near the crack tip. Idealized flexible boundary conditions would move the singularity of the stress field together with the crack tip in the crack propagation direction as the atomic bond breaks and the crack advances. To check the influence of the fixed boundaries on the stability range of the crack, the stability of the medium size system for the (110) crack with [1$\bar{1}$0] front was studied for three different positions of the crack tip with respect to the atomic bond. The different positions are shown in Fig. 4. For the (110)[001] and (111)[0$\bar{1}$1] cracks, where the bonds are perpendicular to the crack plane, it is assumed that the crack tip is located in the middle of a bond.

2.2. Computational method

The energies and atomic forces were calculated within the local density approximation (LDA) to DFT in its plane-wave pseudopotential formulation [24]. Within DFT the determination of the ground state of a system of many interacting electrons and ions is mapped onto a single particle problem with an effective one-body hamiltonian. This hamiltonian contains the usual kinetic energy, ion–electron and Hartree interaction terms plus the so-called exchange–correlation contribution. The exchange–correlation functional is not known exactly, but approximated by the LDA, which usually provides a very good description of the structural and energetic properties of solids. Pseudopotential theory replaces the strong electron–ion Coulomb interaction potential with a much weaker pseudopotential, which effectively includes the Pauli repulsion of the valence and the core electrons.

The supercell approximation allows one to deal

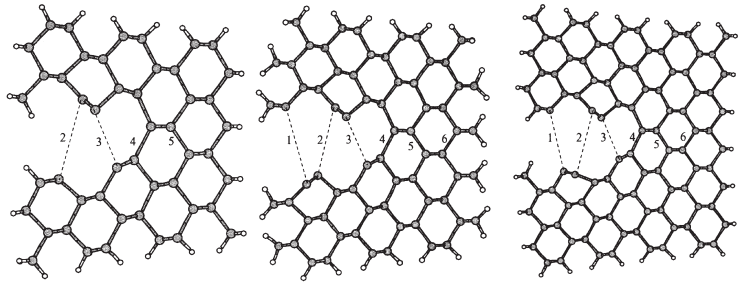

Fig. 2. Relaxed atomic configurations for the different systems sizes of the (110)[1$\bar{1}$0] crack at a stress intensity factor of $K_I = 1.20K_I^G$, where all systems are stable. Details of the different systems are given in Table 1. The bonds across the crack plane are labelled 1–6 for further reference. Dashed lines correspond to broken bonds.

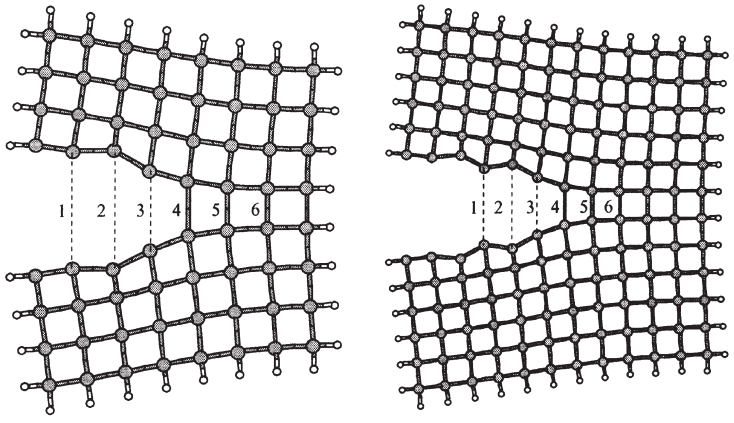

Fig. 3. Same as Fig. 2 but for the (110)[001] crack system.

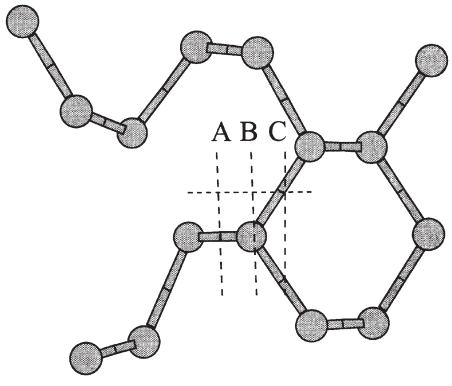

Fig. 4. Different positions of the centre of the elastic field of the crack with respect to the atomic coordinates that have been studied for the (110)[1$\bar{1}$0] crack.

with arbitrary atomic configurations within the framework of Bloch's theorem. The electronic wave functions are expanded in terms of a discrete plane-wave basis set, $\exp[i(\bar{k}+\vec{G})\vec{r}]$, where $\bar{k}$ is a vector in the Brillouin zone and $\vec{G}$ is a reciprocal lattice vector. The number of plane waves included in the calculation is characterized by the cutoff energy, E_{cut}: only plane waves with kinetic energy $(\hbar^2/2m|\bar{k}+\vec{G}|^2$ smaller than the cutoff energy are included in the calculation. This truncation of the plane wave basis leads to errors in the total energy. However, these errors can be controlled directly via the cutoff energy. The sampling of the Brillouin zone is performed using a Monkhorst–Pack $\bar{k}$-mesh of 1×1×4 (two inequivalent $\bar{k}$ points) [27].

The search for the ground state of the electronic system for a given atomic configuration is performed with a direct, completely self-consistent second order search for the minimum of the electronic energy functional, using a conjugate-gradient method. Once the electronic ground state is known, forces on the different atoms are calculated and the atoms are relaxed using a conjugate-gradient minimization. This relaxation of the electronic system and the atoms is repeated until the total energy is converged to 10^{-4} eV/atom and the forces fall below 0.01 eV/Å (0.016 nN) on every atom.

The computational cost of the iterative minimization techniques used to determine the ground state electronic energy scales with N_{PW}, the number of plane waves as $N_{\mathrm{PW}} \ln N_{\mathrm{PW}}$, with $N_{\mathrm{PW}} \propto E_{\mathrm{cut}}^{3/2}$. It is therefore important to keep the cutoff energy as low as possible, without compromising on the quality of the description provided by the pseudopotential. An optimized non-local pseudopotential [28, 29] has been used here for silicon. The *p* and *d* components of the potential are made similar and optimized to make the pseudopotential rapidly convergent with respect to the cutoff energy in the plane-wave expansion. The pseudopotential was applied in a separable form, taking the *p* component as reference and including only the *s* non-local component. The projection of this component was performed in real space [30]. This pseudopotential provides a good description of the structural and energetic properties of Si, as shown in Section 3. A bare Coulomb potential is used for hydrogen.

2.3. Determining lattice trapping

2.3.1. Method for loading/unloading. The Griffith model provides the starting point for our analysis of crack stability. The Griffith stress corresponds to the exact balance between the energy stored in the elastic field of the crack and the energy needed to create the two fracture surfaces. From linear anisotropic elasticity, it is known that the stored elastic energy, $\mathcal{G}$, is proportional to the square of the stress-intensity factor K_{I}^2. Only mode I (opening mode) loading of the crack is considered here. Calculated surface energies are used to determine the values of $K_{\mathrm{I}}^{\mathrm{G}}$ which satisfy the Griffith criterion for the different crack orientations. Table 2 provides all the relevant information for this analysis, including the values of $K_{\mathrm{I}}^2/\mathcal{G}$ (related to the crack geometry and the elastic constants of the material), the surface energy and the

Table 2. Relevant information characterizing the crack systems. The values of $K_I^2/\mathcal{G}$ reflect the elastic anisotropy. The calculated surface energies (in units of eV/Å^2 and J/m^2) are needed to calculate the critical stress intensity factors K_I^G

Crack orientation	$K_I^2/\mathcal{G}$	Surface energy		K_I^G
	GPa	eV/Å^2	J/m^2	MPa$\sqrt{\text{m}}$
(111)[0$\bar{1}$1]	56.21	0.08997	1.441	0.4026
(110)[1$\bar{1}$0]	57.79	0.1082	1.733	0.4476
(110)[001]	51.99	0.1082	1.733	0.4245

resulting critical value for the stress intensity factor K_I^G. The experimental elastic constants of Si [31] have been used for the determination of $K_I^2/\mathcal{G}$.

As discussed in the introduction, experiments and theoretical calculations show a clear deviation from the behaviour predicted by the simple Griffith picture. Cracks can be stable for a range of different strain/stress values around the critical Griffith value, the so-called lattice trapping range. To determine this range, the structure of cracks is studied for different loads above and below the Griffith value, K_I^G.

The initial crack configuration corresponds to the atomic coordinates given by linear anisotropic elasticity theory for a stress intensity factor of 1.0 or 1.2 K_I^G for all the crack orientations considered. The initial configurations are fully relaxed to mechanical equilibrium to determine the crack structure for these loads. All configurations are stable at both loads. The resulting structure with the opened crack is taken as the starting configuration for further loading or unloading: the initial configuration ($\vec{r}_{\text{new}}$) for the new load (K_I^{new}) is determined from the previous relaxed configuration ($\vec{r}_{\text{old}}$) by re-scaling the displacement of the atoms with the ratio of the stress intensity factors, according to:

$$\vec{r}_{\text{new}} = \vec{r}_{\text{ref}} + \frac{K_I^{\text{new}}}{K_I^{\text{old}}}(\vec{r}_{\text{old}} - \vec{r}_{\text{ref}}) \qquad (3)$$

where $\vec{r}_{\text{ref}}$ are the atomic coordinates of the perfect crystal. Note that such scaling is exact within linear elasticity theory. Loads up to 1.5 K_I^G and down to 0.75 K_I^G have been explored in steps of 0.05 K_I^G. We have carefully checked that the loading history does not change the stability of the crack.

2.3.2. Determination of bond distances and $K_I^{+,-}$. The structure of the crack for different loads provides all the necessary information to determine the lattice trapping range. In particular, the behaviour of bond distances across the crack plane as a function of load contains clear features which signal the advance or the receding of the crack. For a given load, bond distances across the crack plane show a very characteristic narrow region, associated with the crack tip, where the bond distance changes abruptly from its value for the bonds in the strained area ahead of the crack tip to much larger values associated with broken bonds. The displacement of the crack can thus be monitored through the changes in bond distances of the bonds close to the crack tip.

Fig. 5 shows bond distances for the large (110)[1$\bar{1}$0] crack system for all the different loads considered in our study. Bond no. 4, the bond closest to the crack tip location in the elastic field, is intact for the initial load of 1.20 K_I^G. It has a length of 2.9 Å and is therefore stretched by almost 25% compared to the bulk value. Bond no. 3 has a bond length of almost 5 Å and is clearly broken. Upon loading the system, the bond distance for bond no. 4 increases smoothly up to a load of 1.35 K_I^G where it increases abruptly from about 3 Å to about 4 Å. This abrupt change is signalling the breaking of this bond and the advance of the crack by one lattice site. This load of 1.35 K_I^G is therefore identified as the upper lattice trapping limit, K_I^+, for this crack orientation. Bond no. 3 shows a similarly abrupt decrease of the bond distance for a load of 0.90 K_I^G — the bond is still marginally stable for 0.95 K_I^G. The abrupt change is related to the re-formation of this bond and the receding of the crack by one lattice site. This load is thus identified with K_I^-. The lattice trapping range ΔK is then defined as $\Delta K = (K_I^+ - K_I^-)/K_I^G$.

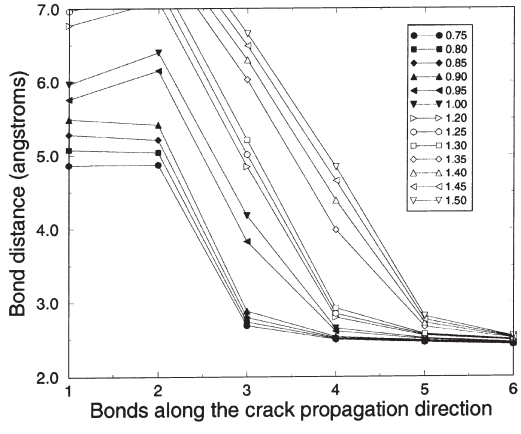

Fig. 5. Bond distances (in Å) for the crack on the (110) plane with a [1$\bar{1}$0] crack front (large system) at different applied loads. The loading is indicated in the legend in units of K_I^G. Bond labels correspond to Fig. 2.

3. SURFACE AND BULK PROPERTIES

3.1. Bulk properties

Table 3 summarizes the relevant bulk properties calculated with our Si pseudopotential and the corresponding experimental data. We have used a cubic cell with eight atoms and a Monkhorst–Pack [27] k-sampling mesh of 4×4×4 to determine the bulk properties. The elastic constants have been determined from fitting to the total energy or to the stress [32] as a function of the strain for different distortions. The values obtained from the two methods differ by less than 0.5%. The agreement between theory and experiment is very good. The remaining differences are common for the DFT–LDA approach we are using [32].

To obtain good quantitative agreement with experiment, the bulk properties are usually calculated with a rather large cutoff energy of 200 eV. Extensive tests on bulk properties and surface reconstructions show that the optimized pseudopotential still gives a good description of Si with as low a cutoff as 96 eV [33]. As an example, we show in Table 3 that the lattice constant and bulk modulus of Si calculated with the 96 eV cutoff compared well with the results for the 200 eV cutoff. For economical reasons, the rest of the calculations in this work are performed with this cutoff energy of 96 eV.

3.2. Surface energies and reconstructions for the Si(111) and Si(110) surfaces

The standard method for calculating the surface energy γ is to evaluate the total energy of a supercell containing a slab with a thickness of a few monolayers and two equivalent surfaces. The surface energy is often determined by subtracting the slab energy from the reference bulk energy, which is obtained from a separate calculation using the bulk unit cell. This procedure does not give accurate results [34, 35], because the comparison of total energies from different unit cell calculations is only accurate if each of the calculations is fully converged in terms of cutoff and k-sampling. However, total energy *differences* between calculations on the same unit cell, where the same cutoff and k-sampling are used, are known to be much less sensitive to these factors. We have therefore followed this second approach and defined the surface energy γ as the difference between the total energy of two calculations in the same supercell: E_{slab} corresponds to the slab, containing N_{slab} atoms, with two surfaces separated by a vacuum region. E_{bulk} corresponds to a calculation in the same supercell, with N_{bulk} atoms, where the vacuum has been filled with Si atoms in order to form a perfectly periodic bulk crystal. The weighted energy of the filled supercell ($E_{\mathrm{bulk}}/N_{\mathrm{bulk}}$) is then taken as the reference bulk energy and the surface energy is defined as:

$$\gamma = \frac{1}{2N_{\mathrm{cell}}}\left(E_{\mathrm{slab}} - \frac{N_{\mathrm{slab}}}{N_{\mathrm{bulk}}}E_{\mathrm{bulk}}\right) \tag{4}$$

where N_{cell} represents the number of atoms in the surface unit cell, and the factor 2 accounts for the two surfaces in the supercell.

3.2.1. Si(111)-2×1 surface. The stable surface structure of the Si(111) surface for $T \leq 600$ K is the 2×1 π-bonded chain Pandey reconstruction [36, 37]. This surface structure is formed during cleavage. The energy released during the bond breaking process allows the system to overcome the small barrier (0.03 eV/surface atom [38]) between the Pandey and the Haneman reconstruction [39], a relaxed structure which can be reached from the ideal (111) surface without an energy barrier. The reconstructed surface is modelled with a supercell containing a Si slab of three {111} double layers of Si with two atoms per layer to account for the 2×1 periodicity. This gives a total of 12 atoms in the supercell. A vacuum region equivalent to three double layer spacings (more than 10 Å) is introduced in the [111] direction. The total energy is calculated using a Monkhorst–Pack (MP) [27] k-mesh of 1×4×2.

An atomic configuration close to the Pandey π-bonded reconstruction was taken as the starting point for the energy minimization. The structural details, including the buckling of the topmost atoms, agree well with other calculations [40]. The difference in height of the two topmost atoms in the reconstruction is quite sensitive to the cutoff of the plane wave expansion. Our optimized pseudopotential produces the correct buckling with the 96 eV cutoff, while standard pseudopotentials require a cutoff larger than 164 eV to recover the correct value.

The relaxed surface energy per surface atom is γ^{111}=1.155 eV/atom (1.44 J/m^2). This result has been obtained using a supercell with the lattice parameter for our Si pseudopotential. Calculations with the experimental lattice parameter change the surface energy only by about 1%. Our surface energy lies between the value estimated from the sublimation

Table 3. Lattice constant (a), bulk modulus (B) and elastic constants of silicon. The results from our calculations with two different cutoffs are compared to the experimental values taken from Ref. [31]

	a (Å)	B (Mbar)	C_{11} (Mbar)	C_{12}	C_{44}
Experiment	5.431	0.992	1.66	0.64	0.80
Calculation (200 eV)	5.461	0.913	1.56	0.59	0.76
Calculation (96 eV)	5.446	0.928	1.53	0.62	

energy [3] (1.46 J/m^2) and the values from other calculations, like non-self-consistent Harris functional calculations with a local orbital minimal basis [25] (1.34 J/m^2) or an empirical tight-binding Green's function approach [41] for an ideal unreconstructed surface (1.36 J/m^2).

3.2.2. Si(110) 1×1 surface. The supercell for the calculation of the (110) surface contains a slab with six (110) planes (two atoms per plane), and a vacuum equivalent to six (110) layers. The reference bulk supercell contains 24 atoms in 12 (110) planes. The total energy is calculated using a MP *k*-mesh of 1×4×2.

While the ideal bulk termination has two surface atoms at the same height (each with a half-occupied dangling bond), the reconstructed surface shows a characteristic buckling of these two topmost atoms. This symmetry breaking is accompanied by a transfer of charge between the atoms in the surface unit cell. The upper atom has a dangling bond occupied by two electrons, while the dangling bond of the lower atom remains empty. This Jahn–Teller distortion opens a gap — the ideal surface with the two equivalent half-occupied dangling bonds is metallic — and further stabilizes the surface structure.

The surface energy is γ^{110}=1.134 eV/atom (1.733 J/m^2). This value is between the few measurements quoted in the literature (1.51, 1.90 J/m^2, see Ref. [25]), and is close to the value of 1.69 J/m^2 obtained for an ideal unreconstructed surface with the empirical tight-binding Green's function approach [41].

In agreement with experimental findings (see the values quoted in Ref. [25]), the surface energy of the (110) surface is larger than the surface energy of the (111) surface.

4. RESULTS FOR FRACTURE SIMULATIONS

4.1. (110) Crack with [1$\bar{1}$0] front

The (110)[1$\bar{1}$0] crack is taken as the test case for which the influence of system size and of the position of the centre of the elastic field is determined. Following the procedure described above we have determined the values of $K_I^{\pm}$ for the medium size system and three different positions of the crack tip (see Fig. 4). The results are summarized in Fig. 6. When the origin of the elastic field is moved across the crack tip bond from A to C, the upper and lower critical loads $K_I^{\pm}$ are both shifted to lower values. However, the lattice trapping range ΔK=0.5 remains almost constant. This indicates that the absolute values of $K_I^{\pm}$ depend on the location of the centre of the elastic field but the lattice trapping range does not. Since our main emphasis will be put on the latter, the choice of the centre of the elastic field is more or less arbitrary. For the rest of this study it is always located at position B.

The dependence of $K_I^{\pm}$ on system size is shown in Fig. 7. The values of $K_I^{\pm}$ are the same for all the sizes, except for a small change of 0.05 K_I^G between the small and the medium size system. This change is of the order of the accuracy of the calculations which, in this respect, is determined by the interval (0.05 K_I^G) by which the loads are changed.

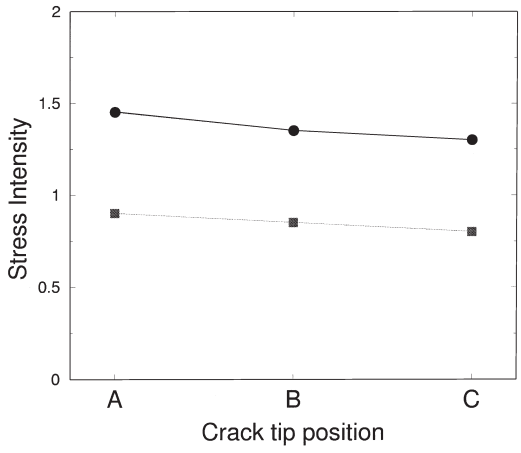

Fig. 6. Lattice trapping range ($K_I^{\pm}$ in units of K_I^G) as a function of the crack tip position of the elastic field with respect to the atomic positions for the (110)[1$\bar{1}$0] crack simulated with the medium size unit cell (see text and Fig. 4 for details).

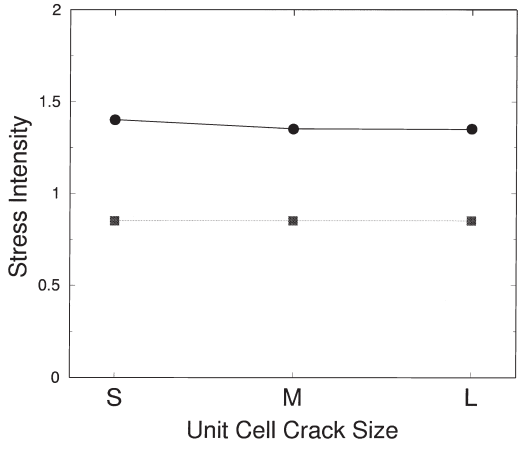

Fig. 7. Lattice trapping range ($K_I^{\pm}$ in units of K_I^G) as a function of the size of the unit cell used to simulate the crack propagation for the (110)[1$\bar{1}$0] crack. S, M and L correspond to the small, medium and large systems for that crack orientation (see Table 1 and Fig. 2). The singularity of the crack elastic field is located at position B with respect to the atomic positions (see Fig. 4).

The bond breaking and healing processes in the (110)[1$\bar{1}$0] crack system are characterized by a pronounced change of the length of the crack tip bond as described in Section 2. The bond breaking process upon loading is analysed in more detail by comparing the bond distances across the crack plane for the medium and large systems in Fig. 8. Both systems show the same general behaviour at the same value of the stress intensity (1.30–1.35 K_I^G). However, the bond length of bond no. 4 before breaking is larger in the smaller system (3.3 Å) as compared to the larger system (3.0 Å). Similarly, the abrupt increase

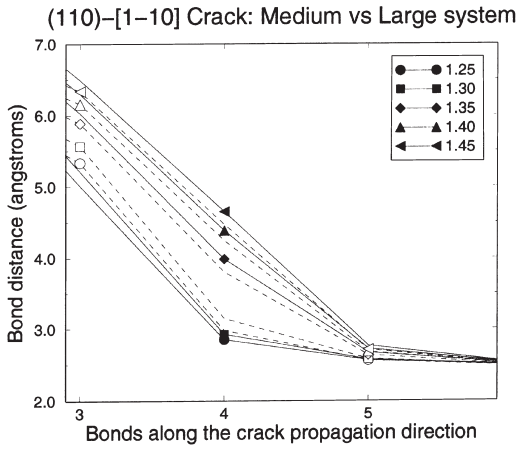

Fig. 8. Comparison of the bond distances (in Å) as a function of stress intensity factor for the medium (dashed lines, open symbols) and large (continuous lines, filled symbols) systems with the (110)[1$\bar{1}$0] orientation.

in bond length of bond no. 4 at a load of 1.35 K_I^G is more pronounced in the larger system. This reflects the less flexible boundary conditions on the crack tip atoms in the smaller systems. Irrespective of these details, the entire bond breaking process is clearly discontinuous at all system sizes.

The atomic configurations immediately before and after the breaking or healing of the crack tip bond are shown in Fig. 9. Note that the breaking of the bonds is accompanied by significant relaxations of the surrounding atoms. Both crack surfaces show the buckling, characteristic of the reconstructed (110) surface. The differences between the medium and large systems for bonds no. 1 and no. 2 are related to this reconstruction of the crack surfaces. The atoms in the lower surface correspond to different buckling orientations in the medium and large system as shown in Fig. 2. It is quite remarkable that the different buckling does not significantly influence crack stability. This is further confirmed by a calculation where one of these atoms is kept fixed at the position given by anisotropic elasticity and its dangling bond saturated with a hydrogen atom. Even such changes do not alter the general behaviour or the critical loads. This insensitivity also explains the very similar results which are obtained for the small system where all these atoms are kept fixed during the relaxation.

4.2. (110) Crack with [001] front

The behaviour of the (110)[001] crack differs significantly from one with the perpendicular propagation direction considered above. Here, the bond breaking process is best described by a "continuous" variation of bond distance with the increase in stress intensity (see Fig. 10). The bond distance of bond no. 4 continuously increases from 3.13 to 4.13 Å with increasing stress intensity. This same general behaviour is observed for both the medium and large system. This continuous behaviour makes the determination of $K_I^{\pm}$ more complicated and $K_I^{\pm}$ not unique. One has to find a critical distance at which the bond is considered broken. The bond distances in this crack system appear to change most significantly after a bond length of 3.5 Å has been overcome. With this criterion, the value of K_I^+ changes from 1.35 to 1.30 K_I^G as the system size is increased from the medium to the large system. However, K_I^-, associated with the healing of bond no. 3, is then equal to 1.00 K_I^G for both sizes. If instead the critical bond distance of the medium size (110)[1$\bar{1}$0] crack system is used, all values drop by 0.05 K_I^G. Consequently the lattice trapping range is not affected by the definition of the critical bond distance and drops from ΔK=0.35 to 0.3 upon increasing the system size from the medium to the large system.

The influence of system size on this crack is also shown dramatically in the behaviour of the system for loads above 1.35 K_I^G: in the large system, the crack propagates further and breaks the next bond (bond no. 5), while the crack in the medium size system does not break bond no. 5 even at 1.5 K_I^G. The atomic configurations for the large system, shown in Fig. 11 for stress intensity factors of 0.95, 1.20, 1.35 and 1.40 K_I^G, illustrate these findings.

4.3. (111) Crack with [0$\bar{1}$1] *front*

The (111)[0$\bar{1}$1] crack system was studied only in the medium system size. The cracks in this system behave qualitatively like the (110)[001] cracks. The bond distances across the crack plane, displayed in Fig. 12, also increase continuously with increasing stress intensity. Depending on the critical bond distance for breaking, the upper and lower lattice trapping limits are 1.25 (or 1.2) K_I^G and 0.90 (or 0.85) K_I^G. The lattice trapping range is again ΔK=0.35.

The atomic configurations at different stress intensity factors (1.20 and 1.25, 1.30 K_I^G) are shown in Fig. 13. For bond distances larger than 5 Å, the fracture surface already develops the Haneman "buckled row" reconstruction. This result agrees with a previous analysis of this reconstruction as a function of the gap distance between the two (111) surfaces [25], which showed that surfaces do not reconstruct for gap distances smaller than 4.6 Å. For distances larger than 4.6 Å the Haneman reconstruction was observed, and it is only for significantly larger distances that the Pandey reconstruction becomes the total energy minimum.

5. DISCUSSION

Fracture processes and the stability of cracks in crystal lattices have so far mainly been studied by empirical atomistic simulation schemes. For silicon this has been done with very simplistic model potentials [4] and more recently also with supposedly more advanced Stillinger–Weber potentials [21]. To the best of our knowledge, there has previously only been one single study of a crack in silicon by more

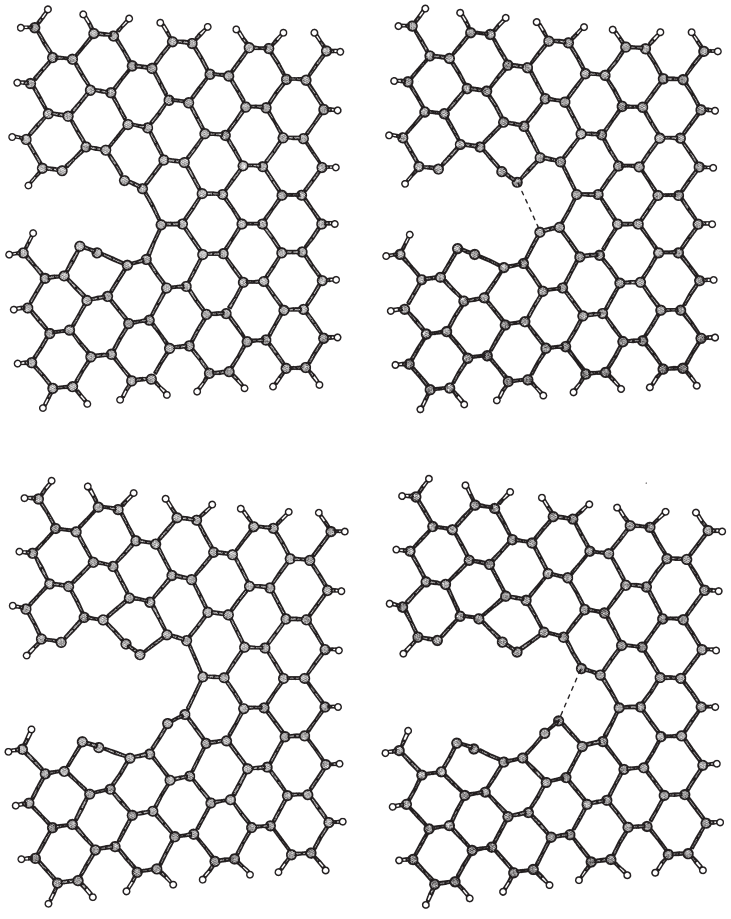

Fig. 9. Atomic configurations (the crack front direction is normal to the plane shown) for the crack on the (110) plane with a $[1\bar{1}0]$ front with different values of the stress-intensity factor: 0.90, 0.95, 1.30 and 1.35 K_I^G. These values correspond to the configurations inmediately before and after the breaking of one of the bonds and the advance of the crack. The broken bonds are marked with dashed lines

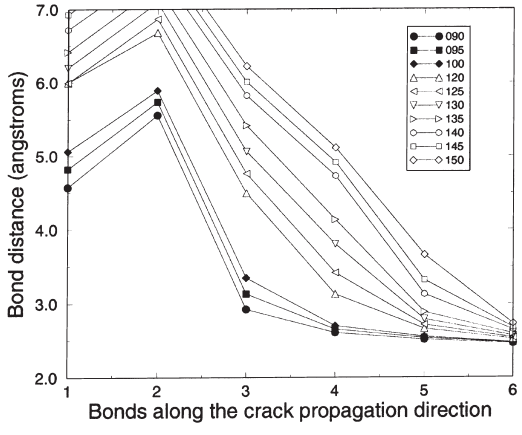

Fig. 10. Same as Fig. 5 but for the crack on the (110) plane with a [001] front. Bond labels correspond to Fig. 3.

advanced quantum mechanical descriptions. This study by Spence *et al.* [25] focused on the $(111)[0\bar{1}\bar{1}]$ crack system only. Our results for the $(111)[0\bar{1}1]$ crack system are compared with these previous studies below.

Sinclair, in his pioneering work [4], explored the influence of the interatomic interaction, described with several simple empirical potentials, on the lattice trapping. He used flexible boundary conditions, where the elastic strain parameters were taken as variables in the minimization process, together with the atomic coordinates in the atomistic region. Sinclair found a lattice trapping range $\Delta K \approx 0.3$–6.0, depending on the model potential used. The larger values were obtained with force laws of shorter range. In comparison with our value of $\Delta K \approx 0.35$ for the $(111)[0\bar{1}1]$ crack system it is obvious that a rigid short range interaction model can not quantitatively account for the crack tip stability in any sense.

The calculations of Spence *et al.* [25] differ from the ones presented here mainly in the quantum mechanical method used for the calculation of the atomic forces. They used a non-self-consistent *ab initio* tight-binding method, based on the Harris functional, with a minimal local orbital basis. Our calculations use a plane wave basis and are fully self-consistent, which provides complete freedom in the determination of the extension and symmetry of the wavefunctions.

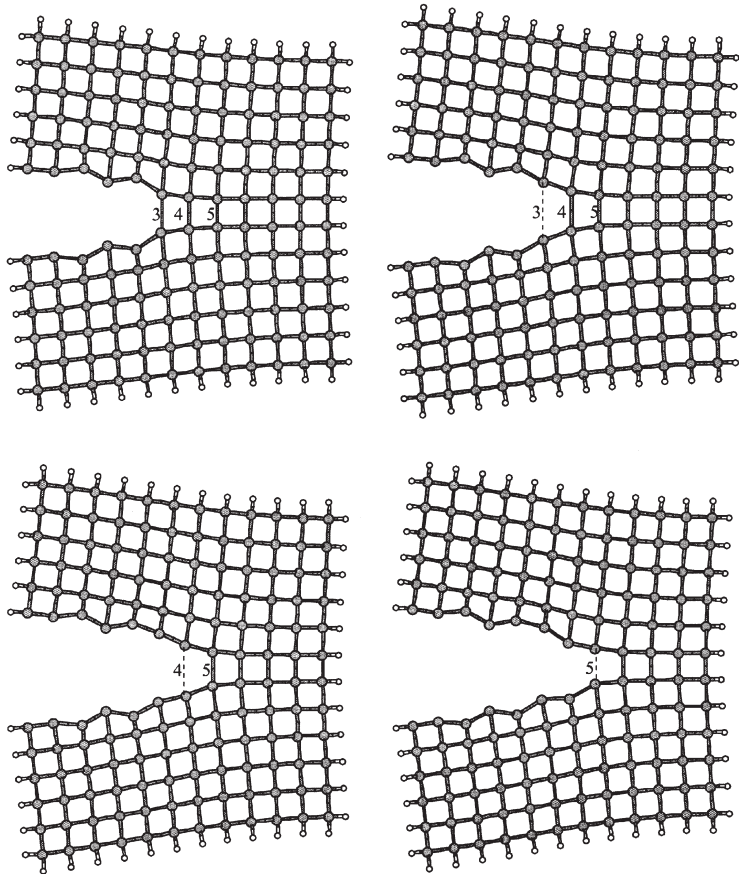

Fig. 11. Atomic configurations (the crack front direction is normal to the plane shown) for the crack on the (110) plane with a [001] front with different values of the stress-intensity factor: 0.95, 1.20, 1.35 and 1.40 K_I^G. The bonds which are broken during the loading process are labelled 3–5 (see Fig. 10). Broken bonds are marked by dashed lines. The origin of the elastic crack field is in the middle of bond no. 4.

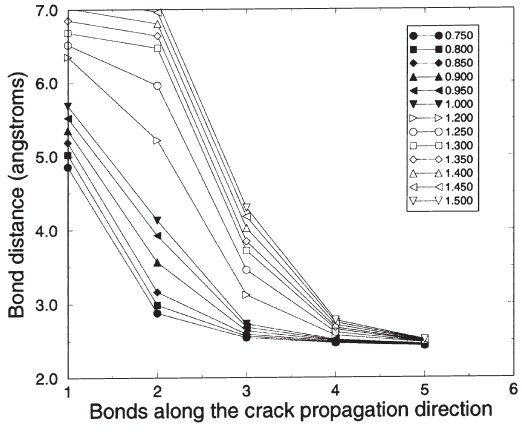

Fig. 12. Same as Fig. 5 but for the crack on the (111) plane with a [011] front. Bond labels correspond to Fig. 13.

Some further differences are the use of isotropic vs anisotropic elastic displacement fields as boundary conditions and somewhat different methods to determine the lattice trapping range. Unfortunately, the different methods to determine the stability range of the crack can hardly be compared. While we determine the bond breaking and healing loads directly by relaxing the entire structures, they computed the energy barrier to crack advance for different values of the stress intensity factor and extrapolate linearly to zero barrier height to determine $K_I^{\pm}$. The energy barriers were determined by computing the total energy for structures which interpolate linearly between two fully relaxed atomic configurations, corresponding to two different positions of the crack tip separated by one atomic increment (one more broken bond). Methodologically their procedure may lead to reasonable estimates for the barrier heights but our method should give more accurate values for the stability limits. At similar system sizes, the magnitude of the lattice trapping range of their calculation ($\Delta K \approx 0.36$) agrees extremely well with our value of $\Delta K \approx 0.35$ for the (111)[01$\bar{1}$] crack system. There are, however, some differences between their neutral load $K_I^{\text{neutral}} = 0.45\ \text{MPa}\sqrt{\text{m}}$, which is defined as the centre of gravity of the stability regime, and the Griffith load to which we have normalized our data ($K_I^G = 0.40\ \text{MPa}\sqrt{\text{m}}$). As a consequence, the absolute values of the loads are slightly different. However, these differences are well within the range in which

the boundary conditions may affect the absolute values.

A second interesting detail in the comparison of the calculations of Spence *et al*. [25] with the study presented here is the dependence of the stability range of the crack on system size. For the (110)[001] crack, which shows the same "continuous" bond breaking process as the (111)[$0\bar{1}1$] crack system studied by Spence *et al*., we have found a decrease in the lattice trapping range with increasing system size. They also find a similar decrease with system size. However, they have addressed the effect of system size with a flexible boundary condition scheme and used a unit cell with 324 atoms divided into two regions: the inner region corresponds to the 120 atoms, which have been used in the fixed boundary calculations and is treated using the *ab initio* tight binding method. The outer region is described by the empirical Tersoff potential. The outer boundary of this region is kept fixed at the elastic solution, while the boundary between the two atomistic regions is flexible, and is determined through a series of minimization steps. These "flexible boundary" calculations gave a slightly different value for $K_{\mathrm{I}}^{\mathrm{neutral}} = 0.47\ \mathrm{MPa}\sqrt{\mathrm{m}}$ but most interestingly also gave a decrease in the lattice trapping range to only $\Delta K \approx 0.27$.

One of the most striking observations in our calculations are the two distinct types of bond breaking processes: a continuous process without pronounced structural relaxations and a clearly discontinuous abrupt bond breaking event. The continuous process, which is observed for both the (111)[$0\bar{1}1$] and the (110)[001] crack systems, mimics what one would expect from continuum theory and therefore results only in a relatively narrow lattice trapping range. The magnitude of the trapping range decreases upon increasing the system size, as detailed above and as also found by Spence *et al*. [25]. Consequently, the trapping in the continuous process may partly be regarded as an effect of the limited system size. One may then conjecture that the trapping range could decrease further upon increasing the system size to macroscopic dimensions. In either case, the low lattice trapping leads to relatively easy propagation of cracks in directions in which this continuous bond breaking occurs. In contrast, the discontinuous process is clearly connected to structural rearrangements in the immediate neighbourhood of the crack tip. Comparing the different system sizes, it is apparent that the lattice trapping is mainly a result of the relaxations of the six to eight atoms immediately surrounding the crack tip. The magnitude of the trapping range therefore does not change with system size even for very small systems. The magnitude of the lattice trapping range connected with this discontinuous bond breaking event (ΔK=0.5) is significantly larger than the trapping range from the continuous process.

The lack of dependence of the trapping range on system size in the (110)[$1\bar{1}0$] crack system is truly remarkable. Even the small system, which only contains 48 Si atoms, of which only 14 are allowed to relax, provides a reasonable estimate of the lattice trapping range. The changes in charge density with stress intensity factor provide an explanation for this behaviour. Fig. 14 shows the charge density in a plane perpendicular to the crack front direction through the crack tip bond for different stages of the loading process for the medium size (110)[$1\bar{1}0$] crack. Marked changes in the electronic distribution are confined to two of the bonds. The one which is breaking and the one immediately above. At a load of 1.25 $K_{\mathrm{I}}^{\mathrm{G}}$, clearly below the critical load, both bonds are significantly weakened to a similar extent. Both do not have a maximum in the charge density in the centre of the bond. As the critical load is approached, the upper bond is recovering charge density at the expense of the crack tip bond and is fully intact again at 1.35 $K_{\mathrm{I}}^{\mathrm{G}}$. Consequently, it appears that a significant part of the lattice trapping in the (110)[$1\bar{1}0$] crack system is caused by the load sharing between the crack tip bond and the one above.

Experimentally, the discontinuous process which is connected to large lattice trapping should result in a relatively high fracture toughness. In contrast, the continuous bond breaking and a small lattice trapping range should lead to low fracture toughness and easy propagation of the cracks. Consequently, the calculations predict a pronounced anisotropy with respect to crack propagation in different directions on the silicon (110) plane. This is in contrast to the thermodynamic Griffith picture where a difference with respect to the propagation direction should only come from elastic anisotropy.

Comparing the calculated propagation anisotropy for {110} cleavage to fracture experiments [16, 42] it seems as if the agreement is only qualitative. Propagation in the "difficult" ⟨001⟩ direction is not seen in experiments, which instead show a deviation of the crack from the original plane onto inclined planes, while crack propagation continues on the {110} plane in the simulations. However, this may well be connected to the boundary conditions imposed on the small atomistic simulation cell which do not favour such deviation of the crack from the original crack plane.

To assess the possibility for the crack to deviate from the original (110) plane, one can compare the opening stress intensity on the (111) plane inclined by Θ=35.3° with respect to the (110)[110] crack with the fracture toughness of the (111)[$1\bar{1}0$] crack system. The inclination of course decreases the opening stress intensity compared to the opening stress intensity on the original (110) plane, however, the large lattice trapping in the "difficult" (110)[$1\bar{1}0$] crack system just compensates this decrease. At the upper lattice trapping limit of the (110)[$1\bar{1}0$] crack system the opening stress intensity on the inclined (111) plane is $K_{\Theta\Theta}(35.3°) = 1.03K^{+}_{(111)[\bar{1}\bar{1}0]}$. The finding that the crack did not deviate, although in principle it could,

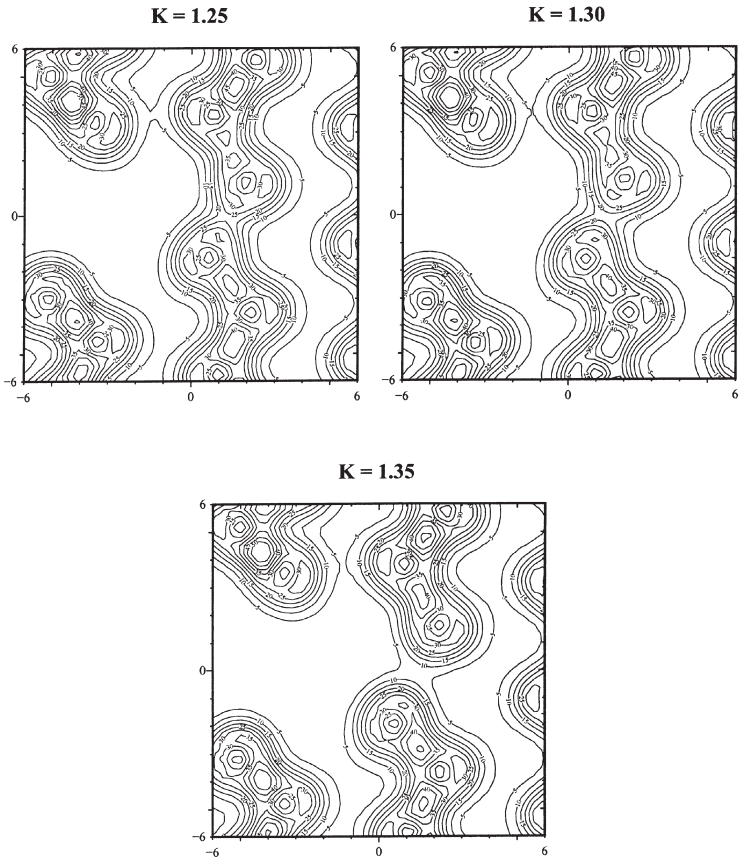

Fig. 14. Charge density plots in a plane perpendicular to the crack front for the medium size (110)[1$\bar{1}$0] crack for three different values of the stress intensity factor (1.25, 1.30 and 1.35 K_I^G). Contours are in units of 10^{-2} electrons/Å^3.

most certainly has to be attributed to the small size of the system.

The inclined crack of course also experiences a mixed mode (opening and shear) loading, which actually exerts a higher driving force on the crack than just the opening component. However, the influence of the mode mixity on the lattice trapping is completely unknown until today and must be deferred to future investigations, which probably require larger system sizes as well. Another aspect which must also be deferred to future investigations is the way in which the lattice trapping barrier can be overcome. The lattice trapping barrier of a crack can be viewed like the Peierls barrier of a dislocation. In analogy to dislocation motion it should therefore be possible to overcome this barrier by the thermally activated generation and motion of kink pairs in the crack front at elevated temperatures. The energetics of this kink pair nucleation process is as yet largely unknown and the study of kink pair formation in a crack front is an important topic for future investigations.

In the comparison to experiment there are two further aspects to be discussed: the first is the magnitude of the critical stress intensity at fracture. Experimental values from static experiments [14] are almost a factor of two higher than the critical stress intensities calculated here. This should probably rather be attributed to the imperfect crack tip geometry and to imperfections in the measured fracture toughness than to possible deficiencies of the calculation, because dynamic fracture experiments indicate that the consumed energy may be as low as 2.5 J/m^2 for the (111) cracks [43] and 3 J/m^2 for the (110) cracks [42], which is in excellent agreement with our calculations. The second aspect raised by the static experiments [14] is which of the cleavage planes of silicon is actually the preferred cleavage plane. Our calculations show a slight preference of the (111) cleavage plane mainly due to its lower surface energy but similar ease of bond breaking for the (110)[001] and the (111)[011] crack systems. However, since the differences in the surface energies are not very pronounced this result has to be regarded with some caution. Specifically, since the absolute values of the lattice trapping for the "easy" directions still seem to depend on system size and therefore remain somewhat unclear.

One of the important side aspects of the present calculations is that the *ab initio* calculations presented here can also provide the basis for the development of future improved empirical potentials for silicon. The results of the crack tip calculations probe the atomic

bonding during the breaking process in a range of distances which is hardly accessible to other calculations and which clearly is of importance for the study of mechanical processes. The calculations therefore can be used as benchmark data which have to be reproduced by a simpler interaction model if an improved potential is to be used in mechanically distorted environments.

6. CONCLUSIONS

Our total-energy pseudopotential calculations show that the bond breaking processes at a crack tip can have very different character. The bond breaking can be continuous — almost as expected from continuum mechanical considerations — or discontinuous. The discontinuous process is clearly connected to atomistic relaxations and rearrangements of only a few atoms around the crack tip. This can partly be understood as a result of some load sharing between the crack tip bond and the neighbouring bond. The discontinuous process results in a rather large lattice trapping as compared to the continuous bond breaking event.

One important consequence of the difference in the bond breaking behaviour is that it introduces an anisotropy with respect to the propagation direction of a crack on one and the same cleavage plane. While bonds break continuously and cracks propagate easily on the {111} plane and the {110} plane if crack propagation proceeds in the ⟨110⟩ direction, a large lattice trapping prohibits crack propagation in a ⟨001⟩ direction on the {110} plane. These differences can explain the experimentally observed anisotropy with respect to propagation direction in silicon single crystals.

Acknowledgements—R. P. acknowledges the financial support from the CICyT (Spain) under project PB97-0028. Computer time on a CRAY T3E was provided at the Computing Centre of the Max-Planck Society.

REFERENCES

1. Griffith, A. A. *Phil. Trans. R. Soc.*, 1921, **221A**, 163.
2. Thomson, R., Hsieh, C. and Rana, V. *J. Appl. Phys.*, 1971, **42**, 3154.
3. Sinclair, J. E. and Lawn, B. R. *Proc. R. Soc.*, 1972, **A 329**, 83.
4. Sinclair, J. E. *Phil. Mag.*, 1975, **31**, 647.
5. Curtin, W. A. *J. Mater. Res.*, 1990, **5**, 1549.
6. Fuller, J. E. R. and Thomson, R. *Fracture*, 1977, **3**, 387.
7. Kohlhoff, S., Gumbsch, P. and Fischmeister, H. F. *Phil. Mag. A*, 1991, **64**, 851.
8. Riedle, J., Gumbsch, P. and Fischmeister, H. F. *Phys. Rev. Lett.*, 1996, **76**, 3594.
9. Perez, R. and Gumbsch, P., *Phys. Rev. Lett.*, 2000, **84**, 5347.
10. Clarke, D. *Semiconductors and Semimetals, Vol. 37*, Academic Press, New York, 1992.
11. Gilman, J. J. *J. Appl. Phys.*, 1960, **31**, 2208.
12. St John, C. F. *Phil. Mag.*, 1975, **32**, 1193.
13. Brede, M. and Haasen, P. *Acta metall.*, 1988, **36**, 2003.
14. Michot, G. *Crystal Properties and Preparation*, 1988, **17-18**, 55–98.
15. Samuels, J. and Roberts, S. G. *Proc. R. Soc. Lond. A*, 1989, **421**, 25.
16. George, A. and Michot, G. *Mater. Sci. Eng. A*, 1993, **164**, 118.
17. Margevicius, R. W. and Gumbsch, P. *Phil. Mag. A*, 1998, **78**, 567.
18. Gumbsch, P. *J. Mater. Res.*, 1995, **10**, 2897.
19. Miller, R., Oritz, M., Phillips, R., Shenoy, V. and Tadmor, E. *Eng. Fract. Mech.*, 1998, **61**, 427.
20. Ortiz, M. and Phillips, R. *Adv. Appl. Mech.*, 1999, **36**, 1.
21. Holland, D. and Marder, M. *Phys. Rev. Lett.*, 1998, **80**, 746.
22. Stillinger, F. H. and Weber, T. A. *Phys. Rev. B*, 1985, **31**, 5262.
23. Tersoff, J. *Phys. Rev. B*, 1988, **38**, 9902.
24. Payne, M. C. et al. *Rev. Mod. Phys.*, 1992, **64**, 1045.
25. Spence, J. C. H., Huang, Y. M. and Sankey, O. *Acta metall. mater.*, 1993, **41**, 2815.
26. Sih, G. C. and Liebowitz, H. in *Fracture*, ed. H. Liebowitz, Academic Press, New York, 1968, pp. 67–190.
27. Monkhorst, H. J. and Pack, J. D. *Phys. Rev. B*, 1976, **13**, 5188.
28. Rappe, A., Rabe, K. M., Kaxiras, E. and Joannopoulos, J. D. *Phys. Rev. B*, 1990, **41**, 1227.
29. Lin, J. S., Qteish, A., Payne, M. C. and Heine, V. *Phys. Rev. B*, 1993, **47**, 4174.
30. King-Smith, R. D., Payne, M. C. and Lin, J. -S. *Phys. Rev. B*, 1991, **44**, 13063.
31. Hirth, J. P. and Lothe, J. *Theory of Dislocations*, 2nd edn. John Wiley and Sons, New York, 1982.
32. Nielsen, O. H. and Martin, M. *Phys. Rev. B*, 1985, **32**, 3780.
33. Perez, R., Stich, I., Payne, M. C. and Terakura, K. *Phys. Rev. B*, 1998, **58**, 10835.
34. Fiorentini, V. and Methfessel, M. *J. Phys. Cond. Matter*, 1996, **8**, 6525.
35. Fiorentini, V. and Methfessel, M. *J. Phys. Cond. Matter*, 1998, **10**, 895.
36. Pandey, K. C. *Phys. Rev. Lett.*, 1981, **47**, 1913.
37. Pandey, K. C. *Phys. Rev. Lett.*, 1982, **49**, 223.
38. Northrup, J. E. and Cohen, M. L. *Phys. Rev. Lett.*, 1982, **49**, 1349.
39. Haneman, D. *Phys. Rev.*, 1961, **121**, 1093.
40. Northrup, J. E., Hybertsen, M. S. and Louie, S. G. *Phys. Rev. Lett.*, 1991, **66**, 500.
41. Berding, M. A., Krishnamurthy, S., Sher, A. and Chen, A. -B. *J. Appl. Phys.*, 1990, **67**, 6175.
42. Cramer, T., Wanner, A. and Gumbsch, P., *Phys. Rev. Lett.*, 2000, **85**, 788.
43. Hauch, J. A., Holland, D., Marder, M. P. and Swinney, H. L. *Phys. Rev. Lett.*, 1999, **82**, 3823.